Morphology of the Red Rectangle Proto-Planetary Nebula

N. Koning

Department of Physics & Astronomy, University of Calgary, Calgary, Alberta, Canada T2N 1N4

nkoning@iras.ucalgary.ca

Sun Kwok

Department of Physics, University of Hong Kong, Pokfulam, Hong Kong, China

sunkwok@hku.hk

W. Steffen

Intituto de Astronomía Universidad Nacional Autónoma de México, C.P. 22860, Ensenada, México

wsteffen@astrosen.unam.mx

ABSTRACT

The morphology of the Red Rectangle (RR) exhibits several singular attributes. Most prominent are a series of linear features perpendicular to the symmetry axis which appear as "ladder rungs" across the nebula. At the edge of each "rung" gas seemingly flows from bright knots in a parabolic shape towards the center of the nebula.

We present a new model of the RR which explains these features as a projection effect of the more common concentric arcs seen in other PPNs (e.g. Egg Nebula). Using the 3D morpho-kinematic modeling software SHAPE, we have created a model of the RR that consists of spherical shells evacuated by a biconical outflow. When the symmetry axis is oriented perpendicular to the line of sight, the spherical shells become linear thereby reproducing the "rungs" seen in the RR. When oriented at different inclinations, the linear features become spherical as observed in the Egg Nebula. The model also accurately reproduces the bright knots and the parabolic outflows from these knots that have proven difficult to explain in the past. Using this model, we are able to place a lower limit on the speed of the outflow of $\sim$158 km s^{-1}.

Subject headings: stars: AGB and post-AGB — stars: circumstellar matter

1. Introduction

The Red Rectangle (RR) nebula is a reflection nebula associated with the late-type star HD 44179. Its peculiar structure, first identified by Cohen et al. (1975), has sparked over three decades of intense study. High resolution Hubble Space Telescope (HST) images of the nebula by Cohen et al. (2004) has raised more questions than they have answered (Figure 1).

The RR has a remarkably different morphology at wavelengths either side of 540 nm. At wavelengths below this cutoff, the nebula is dominated by dust scattering and the Blue Luminescence (Vijh et al. 2004) peaking at 380 nm. The resulting morphology at these lower wavelengths is largely spherical. At wavelengths longer than 540 nm, the luminosity of the RR is dominated by the Extended Red Emission (ERE) which gives the nebula its distinctive red coloring (D'Hendecourt et al. 1986). The morphology at these longer wavelengths will be the focus of this paper (Figure 1).

On a general level, the RR has a bipolar morphology similar to many other bipolar planetary nebulae (PNs) and proto-planetary nebulae (PPNs). However, the RR also has a host of attributes rarely seen in other objects. First, the bi-cone "X" shape of the nebula differs from typical PNs and PPNs, which are more likely to have curved bipolar lobes. On the surface, the straight, sharp walls of the bi-cone suggests an ejection mechanism, perhaps by a bipolar jet (Morris 1981) caused by binary interactions, or a bi-conical outflow driven by radiation pressure (Icke 1981, 2003). Second, bright knots appear along the walls of the bi-cone and seem to be associated with gas streaming away from the edge of the wall. Third, each knot appears to be connected to another on the opposite wall of the bi-cone by linear features dubbed the "ladder rungs" by Cohen et al. (2004). The "rungs" represent a major hurdle in the explanation of the formation of this nebula.

In 2007, Tuthill & Lloyd (2007) reported observations of a nebula around the star MWC 922 that shares these rare attributes. Dubbed "The Red Square", this nebula reveals that the observed morphology of the RR is not unique and may simply be due to a rare, but fortuitous viewing angle.

The first question that faces us is whether the RR Nebula is or is not part of the general phenomenon of PPNs. Many PPNs have bipolar structures with sharp boundaries, properties that are shared by the RR Nebula. The regularity of the "ladder rungs" suggests a periodic phenomenon, which has also been observed in other PPNs as multiple concentric circumstellar arcs. The best observed example of these circumstellar arcs is in the Egg Nebula (AFGL 2688, Sahai et al. 1998), but they are also seen in many bipolar PPNs (Kwok et al. 1998; Kwok, Su, & Stoesz 2001). An HST image of the Egg Nebula is shown in Figure 2. The two pairs of "search light beams" and the multiple arcs are all due to scattered light.

Up to 23 arcs can be seen extending all the way to the outer regions of the "beams". The multiple arcs are projections of 3D shells onto the plane of the sky and illuminated within the bipolar lobes by visible photons from the central star(s). The bright boundaries towards the center of the nebula represent the surfaces of conic cavities carved out by bipolar outflows from the central star. The "beams" emanate from the tips of these cavities.

Bi-conic structures are also observed in PNs. The well-known Dumbbell Nebula (NGC 6853), in spite of its name, actually has a triple bi-conic structure with a bipolar axis inclined at 15° from the plane of the sky (Kwok et al. 2008). The dynamical ages of the triple cones are of the order of several hundred years, similar to the dynamical ages observed in circumstellar arcs. It is suggested that even the famous Ring Nebula (NGC 6720) has a similar intrinsic triple cone structure. Further evidence of bi-conic structures are demonstrated in the PNs Hb12 (Kwok et al. 2007), MyCn18 (Sahai et al. 1999) and He2-104 (Contini et al. 2001) (Figure 3). Due to their inclination, this bi-conic structure manifests itself as curved "etchings" along the walls of the bi-polar lobes.

If we examine the periodic structures observed in the RR Nebula with those seen in bipolar PPNs, the major difference is that the structures, instead of being curved arcs, are straight lines. In this paper, we explore the possibility that the RR Nebula shares the same intrinsic 3D structure as other bipolar PPNs such as the Egg Nebula, and that the different apparent morphology is solely the result of orientation.

2. The Model

Modeling of the RR was accomplished with the software SHAPE; a morpho-kinematic modeling program for the reconstruction of gaseous nebulae (Steffen et al. 2010). SHAPE is a suitable choice for modeling the structure and radiation transfer of PPNs since it can simulate scattering from a central source and seamlessly create complex 3D geometries with equally complex density. The SHAPE RR model consists of a spherical halo consisting of two components (ERE and dust), a bi-conical cavity and a central illuminating source.

2.1. Geometry

The distance to the RR is uncertain, but for this work we adopt the value of 710 pc deduced by Men'shchikov et al. (2002). The model consists of a central illuminating source (star) surrounded by a spherical halo of dust with radius $r = 1.27 \times 10^{17}$ cm . The radius of the dust distribution is cut-off at this value in order to save computation time. The halo

has a radial number density profile of $n \propto r^{-2}$ where r is the distance from the center of the nebula. Both the ERE and dust component are spatially mixed and share this density profile. The SHAPE mesh model of this geometry is shown in Figure 4

The dusty halo contains spherical shells of increased density to simulate mass ejection events. The density enhancements are Gaussian in shape with an amplitude of 1 and a FWHM of 0.47. The central positions of the enhancements follow the measured values of the ladder rungs by Cohen et al. (2004) for the northern lobe and are listed in Table 1. A graphical representation of the integrated density is shown in Figure 5.

The second component to the geometric model is a bi-conical cavity. Each cone has a length of 1.38×10^{17} cm, a maximum radius of 7.97×10^{16} cm and a minimum radius of 3.82×10^{15} cm (255 AU). Although Men'shchikov et al. (2002) suggest an inner radius for the torus of 14 AU (our minimum radius of the cones), the spatial resolution of our grid (256^3) is not enough to resolve this structure. The effective opening angle of the cones is 57.6°. The bi-cones have an inclination of 0° and a position angle of -15°. The cavity is completely void of any dust and therefore the light from the central star can freely propagate throughout this region and only diminishes as r^{-2} due to geometric dilution.

2.2. Central Star

The central star (HD 44179) of the RR has a temperature of T=8250K and a luminosity of $L \sim 6000 L_{\odot}$(Vijh et al. 2005) and is not sufficiently hot to ionize the surrounding gas. Emission from the gas component is therefore non-existent. These values are used for the central source in our SHAPE model.

2.3. ERE Component

ERE is a photo-luminescence process associated with dust in the ISM (Witt et al. 2006). In addition to the RR, ERE has been observed in reflection nebulae (Witt et al. 1984; Witt & Boroson 1990), H II regions (Perrin & Sivan 1992; Darbon et al. 2000), and the galactic halo. The carrier of the ERE is not known but many possibilities have been suggested in the literature including silicon nanoparticles (Witt et al. 1998; Ledoux et al 1998), neutral PAH molecules (D'Hendecourt et al. 1986), PAH clusters (Seahra & Duley 1999) and Hydrogenated Amorphous Carbon (e.g., Witt & Schild 1988). Witt et al. (2006) suggest the ERE is generated in a two step process where photons with energy > 10.5 eV creates the ERE carrier from some precursor and lower energy UV/optical photons excite

the carrier which leads to the ERE. Witt et al. (2006) conclude that the most likely carrier of the ERE is doubly ionized PAH molecules.

In order to investigate the morphology of the RR, in SHAPE we must simulate the emission of the ERE by dust. We are not interested in the details of the carrier, only in the resulting morphology. Several key features of the ERE are thus important to this study:

1. The intensity of the ERE is dependant on the density of the local radiation field (Gordon et al. 1998)
2. Photo-luminescence is linearly proportional to the density of the carrier
3. The ERE has an isotropic radiation pattern (Witt & Vijh 2004)
4. The ERE in the RR extends from 540 nm to 750 nm (Schmidt et al. 1980)
5. The ERE absorbs primarily at wavelengths smaller than 170 nm. (Witt & Vijh 2004)

The first three items are shared with a typical scattering process where the phase function is isotropic. This allows us to simulate the ERE with a modified scattering algorithm. The fourth item suggests how the scattering algorithm must be modified. Schmidt et al. (1980) provide a high resolution spectrum of the RR over the wavelengths from ∼450 nm - ∼750 nm (Figure 6). We find that if we invert the spectrum and assign the resulting values to the scattering coefficient (multiplied by the density and a scaling factor) we are able to reproduce the wavelength dependence of the ERE for the RR (Figure 7).

2.4. Dust Component

The spherical glow of the RR at wavelengths shorter than 540 nm necessitates an additional dust component that scatters light from the central star (in this model we focus on wavelengths longer than 450 nm and are therefore not concerned with the Blue Luminescence which dominates ∼380 nm). We require the dust to be optically thin at wavelengths $<$ 540 nm in order to produce the necessary spherical halo even within the equatorially dense region. Decreasing the density of the dust not only drops the opacity (as required) but also lowers the intensity of the scattered light, so this is not a trivial requirement. We find that due to the low absorption index of silicates over the wavelengths of interest (Krugel 2003), dust composed of small silicate grains may be optically thin even when densities are high enough to produce the necessary illumination.

The dust is therefore made up of silicate grains with a radius of 10 nm and optical constant (n and k) given by Krugel (2003). The scattering and absorption coefficients are calculated using Mie Theory. In order to match the relative intensity of the blue component of Figure 6, the dust density is required to be 100x greater than the ERE component.

2.5. Radiative Transfer in SHAPE

Radiative transfer in SHAPE is accomplished through a ray-casting algorithm. The aforementioned 3D model is subdivided into a 256^3 -cell grid; each cell representing a volume through which radiative transfer is performed. The first step is to cast a ray from the central star outwards to every cell. Each ray consists of 100 spectral bands ranging from 400 nm to 700 nm. Radiative transfer is carried out along this ray (using the absorption and scattering coefficients mentioned above) and a final scattered intensity is derived for each cell. Then, for each pixel in the final image, another ray is cast from the back towards the observer and radiative transfer is performed once again over each cell. Once ray casting is complete, the intensity of each emerging ray is assigned to a pixel on the final image.

3. Results

The model described above is rendered at 467 nm and 622 nm and compared to HST images of the same wavelengths in Figure 8. The model rendered over the entire 400 nm 700 nm range and compared with the equivalent HST image is displayed in Figure 9. The color scale for each image in Figure 9 is the same.

The model image at 467 nm shows the spherical glow seen in the HST image. This glow is caused by the scattering of small, optically thin silicate dust grains. The remainder of this analysis will concentrate on the morphologically more interesting longer wavelength images dominated by the ERE. Clearly visible are several key features of the RR Nebula. Foremost is the characteristic X shape of the nebula. This is a natural consequence of light from the star scattering off the inner edge of the bi-cone geometry. The reason the edges are enhanced is because it is in this direction that we are looking through the most material.

Also notable in the model image is the presence of linear features spanning the bi-cone lobes. These features are obviously a purely optical effect as no such geometry was built into the model. Since the spherical dusty halo has been evacuated within the bi-cone, what remains of the density enhancements (spherical shells) in this region is a thin circular etching of dust on the walls. When seen almost exactly edge on, these etchings appear linear

in nature and naturally explain the "ladder rungs" seen in the RR.

The bright knots that appear to connect the ladder rungs to the walls of the nebula are also evident in the model image. The cause of the bright knots is also an optical effect due to our fortuitous edge on view of this nebula. The reason we see the "ladder rungs" is the same reason we see these bright knots. The etchings of the density enhancements left on the wall of the bi-cone are seen edge on. We see through more of the material at the tips of the ring and therefore they appear brighter, producing the observed knots.

By following this line of reasoning, an explanation for the flowing of gas from these knots is apparent. The walls of the bi-cone are not completely opaque, and light from the star can penetrate slightly into the dusty halo illuminating some of the dust. Outside the bi-cone cavity, the dust remains in a spherical geometry and hence we see "extensions" from the walls that seem to flow backward. In our model, these extensions are spherically concentric around the central star, however in the RR they are rather parabolic. To explain the parabolic shape in our scheme, we propose that the original spherical shells have been accelerated by the outflow that created the bipolar cavity. Since the acceleration diminishes with distance from the edge, the shape of the extensions take on a parabolic shape.

To demonstrate the illusion of the "ladder rungs" and the knots, we have created several images of the model at different inclinations in Figure 10. As the inclination increases, we clearly see the ladder structure give way to the more commonly observed concentric arcs. This is because the wall etchings are no longer seen edge on, and we begin to see their true curvature. Similarly, as the inclination increases we no longer see through the edge of the etchings and therefore the knots begin to fade.

Figure 11 shows a model image of the RR at an inclination of 30° (left panel). The etchings on the inner walls of the cavity strongly resemble conical structures at this inclination. Hb12 (right panel) is a PN and therefore emits via ionization so we can not directly compare it to our scattering model. However, when ionized, our model structure may naturally explain the conic etchings seen in Hb12.

4. Discussion

Previous models of the RR Nebula (e.g., Icke 2003) concentrate on the dynamical aspects and how dynamical events can create the observed structure. In this study, we have emphasized the radiative contributions to the morphological structure of the nebula. The bright "ladder rungs" are not the result of physical ejection events, but are in fact projections of spherical shells outside of the conical cavity. Since light in PPNs and reflection nebulae

is due to scattering and not from direct emission (as in the case of recombination lines and collisionally excited lines in PNs), the optically bright region of a PPN in fact represents a volume where light can escape rather than regions of high density (Kwok 2004, 2010). If the "ladder rungs" are the result of physical ejections, it would be extremely difficult to devise a mechanism that can result in such a morphology. Our model naturally explains the unique morphology of the RR Nebula in terms of a universal bipolar model showing that the RR Nebula "rungs" are no different than the concentric arcs in the Egg Nebula.

We can use this model to determine some properties of the evacuating mechanism that created the bi-cone cavity. The innermost "ladder rung" is located at 2.03×10^{16} cm from the center of the nebula. The exact expansion speed of the "rung" is not well known, but for this analysis we will assume a velocity of 7 km s^{-1} (Cohen et al. 2004). This then suggests that the closest rung is $(2.03 \times 10^{16}$ cm$)/(7$ km s$^{-1}) \simeq 920$ yr old. Since this inner "rung" is linear and not circular, the evacuating mechanism must have been active less than 920 years ago. This gives us an upper limit on when the mechanism shut off.

The furthest "rung" observed by Cohen et al. (2004) is at a distance of 4.57×10^{17} cm. Assuming the evacuation occurred after all the ejection events where complete, the evacuating mechanism must have been able to reach this outer "rung" in under 920 years indicating a minimum velocity of 4.57×10^{17} cm/920 yr $\simeq 158$ km s^{-1}. This value is in agreement with Witt et al. (2009) who place an upper limit on the speed of the outflow of 560 km s^{-1}. The lower limit on the outflow speed derived here depends, of course, on accurate distance measurements and our ability to see fainter "ladder rungs". Using the maximum speed derived by Witt et al. (2009), we can predict that we should not see any "rungs" further than 560 km s$^{-1}\times$ 920 yr $\simeq 1.6 \times 10^{18}$ cm, or about 150″ from the center of the nebula.

5. Conclusions

The RR nebula is modeled by a multiple-shell spherical dust envelope whose central part is carved out by a hollow cone. The observed structure of the nebula is created by star light escaping through the cavity illuminating the walls of the cones. By using this model to fit the observations, we can draw several conclusions about the structure of the RR Nebula and the mechanism that created it:

1. The RR Nebula is formed by an outflow that created a bi-cone cavity void of dust. The reflected light off the walls of the cavity gives rise to the characteristic X shape.

2. The peculiar "ladder rungs" are in fact projections of more familiar concentric arcs seen edge on. The arc structure within the cone is destroyed by the outflow, leaving behind a circular etching within the walls of the cavity. These etchings take on a linear appearance when viewed edge on.

3. The bright knots connecting the "rungs" to the bi-cone walls are a result of seeing the etchings edge on as we look through more material at their tips.

4. The outflow of gas emanating from the knots is nothing more than an extension of the concentric arcs seen outside the bi-cone cavity.

5. The outflow that created the nebula must have ended no more than 920 years ago.

6. The velocity of the outflow is greater than 158 km s^{-1}.

7. No "ladder rungs" should be visible beyond 150″ from the center of the nebula (assuming the upper limit on the outflow velocity derived from Witt et al. (2009))

This exercise demonstrates that the appearance of the optical morphology may not be a tracer of matter distribution, but represents an interaction between radiation and matter. By using a 3D model, we can determine the intrinsic structure of the nebula and show that some features of the RR morphology are no different from other bipolar PPNs such as the Egg Nebula. The basic structure of both objects is due to the collimated fast outflows carving out a central bipolar cone from a pre-existing spherical nebula. The odd ladder rung morphology of the RR is a consequence of the interaction between these outflows and the concentric arcs combined with our fortuitous viewing angle. Our geometric model is therefore useful in constraining the dynamical processes that are responsible for the interaction between the AGB stellar wind and the post-AGB fast directional outflow.

NK acknowledges support from the Natural Sciences and Engineering Research Council of Canada (NSERC), the Alberta Ingenuity Fund and the Killam Trusts. This work was supported by a grant to SK from the Research Grants Council of the Hong Kong Special Administrative Region, China (Project No. HKU 7031/10P). WS acknowledges support by grants from CONACYT 49447 and UNAM PAPIIT IN100410.

REFERENCES

Cohen, M., et al. 1975, ApJ, 196, 179-189

Cohen, M., Winckel, H.-V., Bond, H.-E., & Gull, T. R. 2004, AJ, 127, 2362-2377

Contini, M., & Formiggini, L. 2004, A&A, 375, 579-583

Darbon, S., Zavagno, A., Perrin, J.-M., Savine, C., Ducci, V., & Sivan, J.-P. 2000, A&A, 364, 723

D'Hendecourt, L.B., Leger, A., Olofsson, G., & Schmidt, W. 1986, A&A, 170, 91-96

Icke, V. 1981, ApJ, 247, 152-157

Icke, V. 2003, IAU Symposium 209, Planetary Nebulae: Their Evolution and Role in the Universe, eds. S. Kwok, M. Dopita and R. Sutherland, pp. 495.

Gordon, K.D., Witt, A.N., & Friedmann, B.C. 1998, ApJ, 498, 522

Krugel, E., The Physics of Interstellar Dust, Institute of Physics Publishing, 2003.

Kwok, S., Su, K.-Y.-L., & Hrivnak, B.-J. 1998, ApJ, 501, L117

Kwok, S., Su, K. Y. L., Stoesz, J. A., 2001, in in Post-AGB Stars as a Phase of Stellar Evolution, ed. Szczerba & Górny, S. K., 115

Kwok, S., Dopita, M., & Sutherland, R. 2003, aspc, 2003, 495

Kwok, S., 2004, in Asymmetrical Planetary Nebulae III: Winds, Structure and the Thunderbird, ed. Meixner, M., Kastner, J. H., Balick, B., & Soker, N. 580

Kwok, S., & Hsia, C.H. , 2007, ApJ, 660, 341-345

Kwok, S., Chong, S.-N., Koning, N., Hua, T., & Yan, C.-H. 2008, ApJ, 689, 219

Kwok, S. 2010, PASA, 27, 174

Ledoux et al. 1998, Astronomy and Astrophysics, 333, L39

Men'shchikov, A.-B., Schertl, D., Tuthill, P.-G., Weigelt, G., & Yungelson, L.-R. 2002, a&a, 393, 867-885

Morris, M. 1981,ApJ, 249, 572-585

Perrin, J.-M., & Sivan, J.-P. 1992, A&A, 255, 271

Sahai, R., et al. 1998, ApJ, 493, 301

Sahai, R., et al. 1999, AJ, 118, 468-476

Schmidt GD, Cohen M, Margon B. ApJ 1980; 239: L133-8.

Seahra, S. S., Duley, W. W. 1999, ApJ, 520, p. 719-723

Steffen, W., Koning, N., Wenger, S., Morisset, C.,& Magnor, M. 2010, IEEE Transactions on Visualization and Computer Graphics (in press)

Tuthill & Lloyd. 2007, SCIENCE, 316, 247.

Vijh, Uma P., Witt, Adolf N., Gordon, Karl D. 2004, APJ, 606, p. L65-L68

Vijh, Uma P., Witt, Adolf N., Gordon, Karl D. 2005, APJ, 619, p. 368-378

Vijh, Uma P., Witt, Adolf N., York, Donald G., Dwarkadas, Vikram V., Woodgate, Bruce E., Palunas, Povilas. 2006, APJ, 653, p. 1336-1341

Witt, A. N., Schild, R. E., & Kraiman, J. B. 1984, ApJ, 281, 708

Witt, A. N., Schild, R. E. 1988, ApJ, 325, p. 837

Witt, A. N., & Boroson, T. A. 1990, ApJ, 355, 182

Witt, A. N., Gordon, K. D., Furton, D. G. 1998, ApJ Letters, 501, p. L111

Witt, A.N., Vijh, U.P. 2004, Astrophysics of Dust, ASP Conference Series, Vol. 309, p.115

Witt, A.N., Gordon, K.D., Vijh, U.P., Sell, P.H., Smith, T.L., & Xie, R. 2006, ApJ, 636, 303-315

Witt, A.N., Vijh, U.-P., Hobbs, L.-M., Aufdenberg, J.-P., Thorburn, J.-A., & York, D.-G. 2009, ApJ, 693, 1946-1958

Enhancement Number	Gaussian Center(arcsec)
1	1.91
2	2.18
3	2.94
4	3.47
5	4.05
6	4.92
7	6.99
8	8.20
9	10.03

Table 1: Gaussian properties of the density enhancements in the dust halo of the RR model. The center values are from Table 3 of Cohen et al. (2004) for the northern lobe.

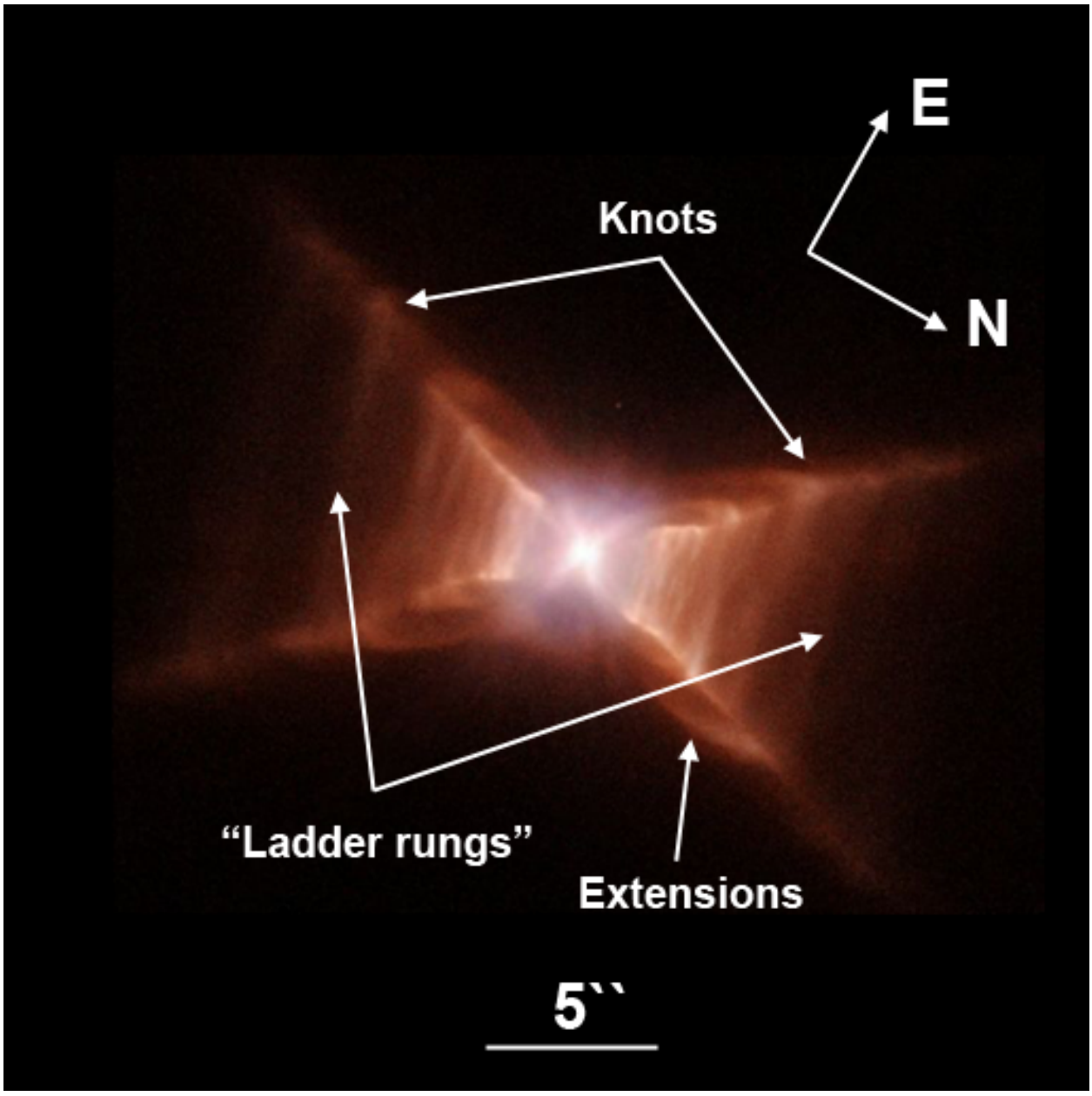

Fig. 1.— HST false-color image of the Red Rectangle. Examples of several "ladder rungs", "knots" and extensions are marked. Image credit: H. Van Winckel, M. Cohen, H. Bond, T. Gull, ESA and NASA.

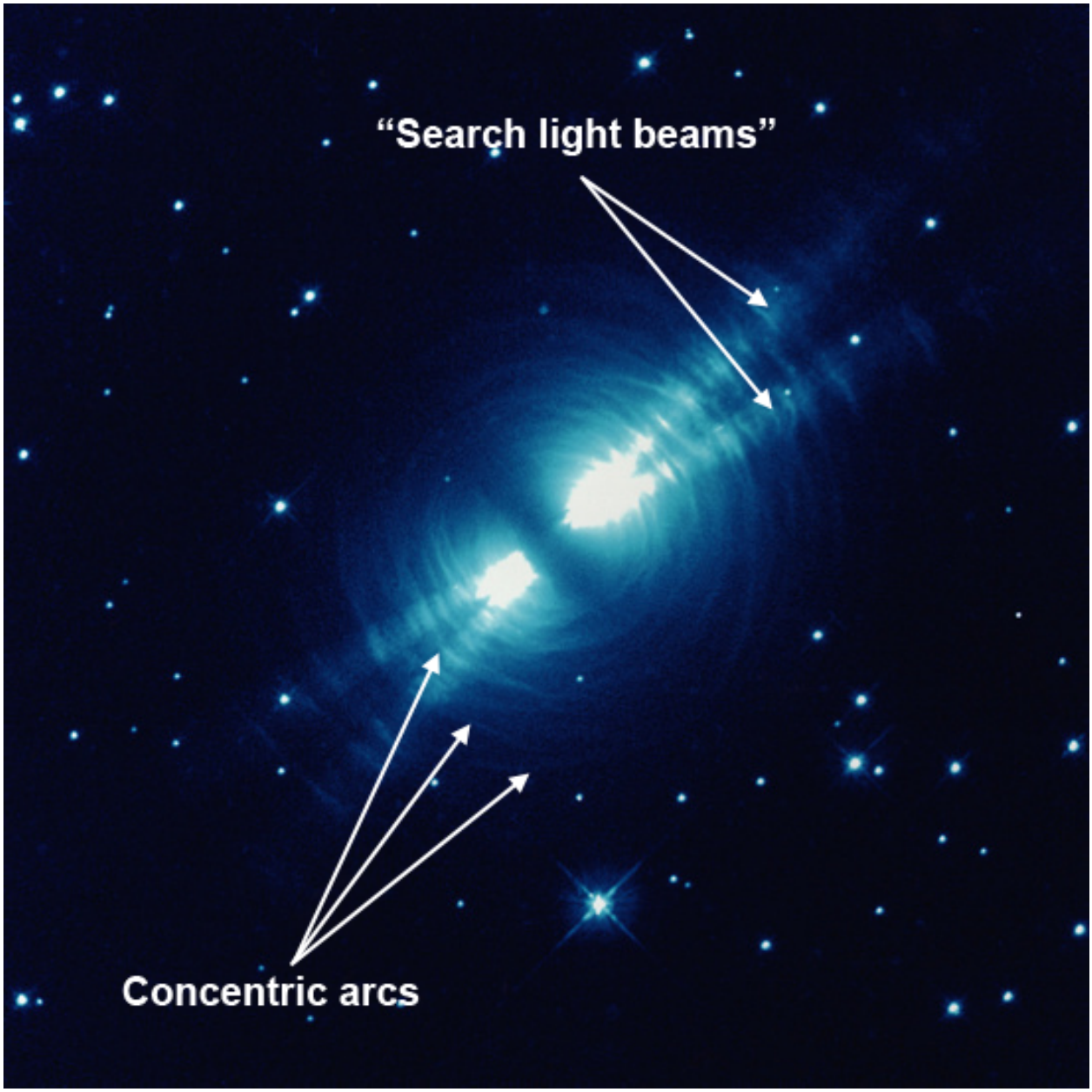

Fig. 2.— HST false-color image of the Egg Nebula. Concentric circular arcs are clearly visible, indicating the existence of periodic phenomena in the nebula. The "search light beams" and some of the concentric arcs are marked. Image credit: R. Sahai, J. Trauger, WFPC2 Science Team, and NASA.

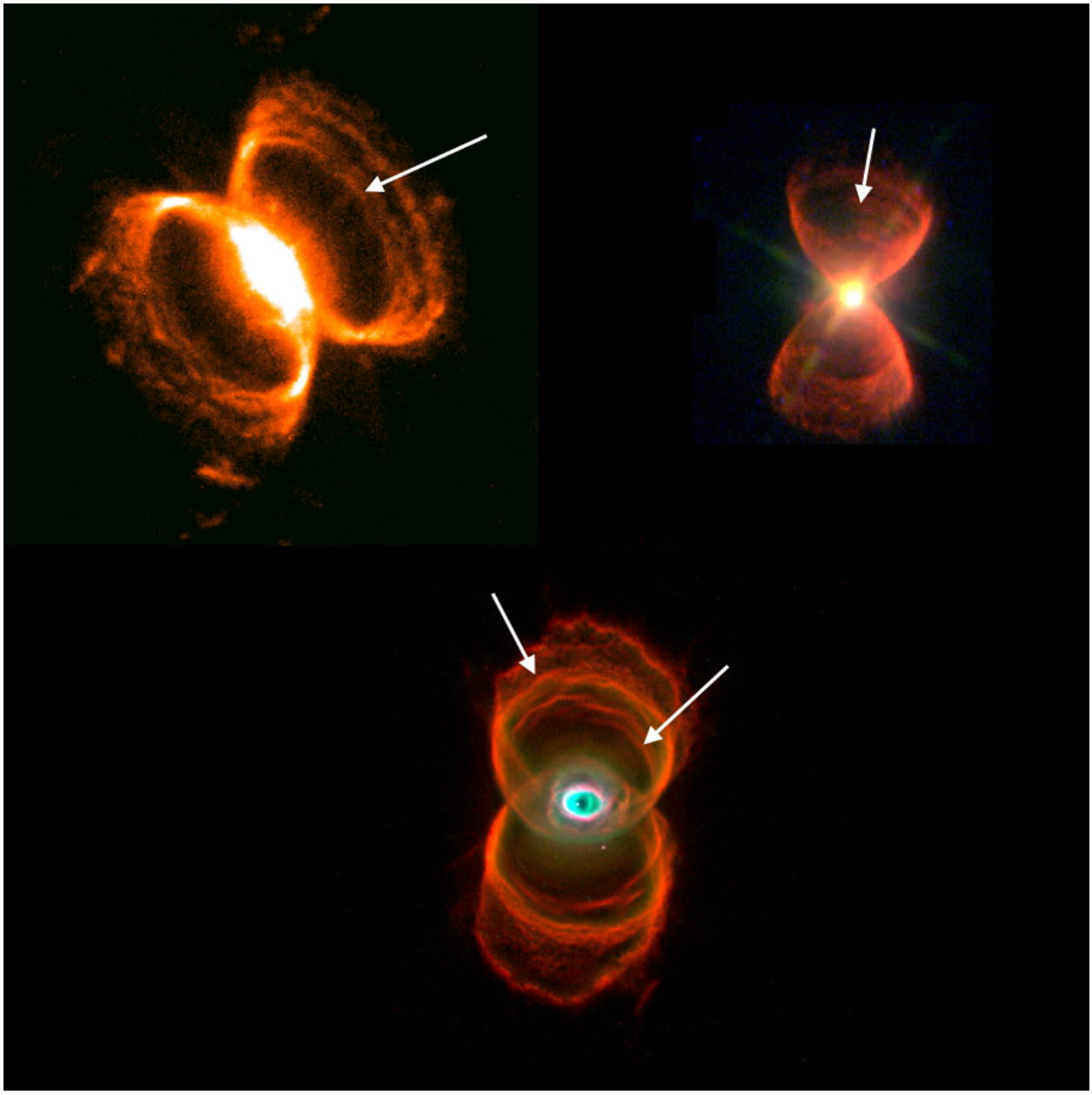

Fig. 3.— Several PNs that exhibit bi-conic structures and conical "etchings" (arrows point to some examples). Top left: HST image of Hen 2-104 (Southern Crab). Credit: PI: Corradi G09336, NASA/ESA/STScI, Hubble Archives. Top right: HST image of Hubble 12. Credit: PI: Balick G09050, NASA/ESA/STScI, Hubble Archives. Bottom: HST image of MyCn18. Credit: Raghvendra Sahai and John Trauger (JPL), the WFPC2 science team, and NASA/ESA

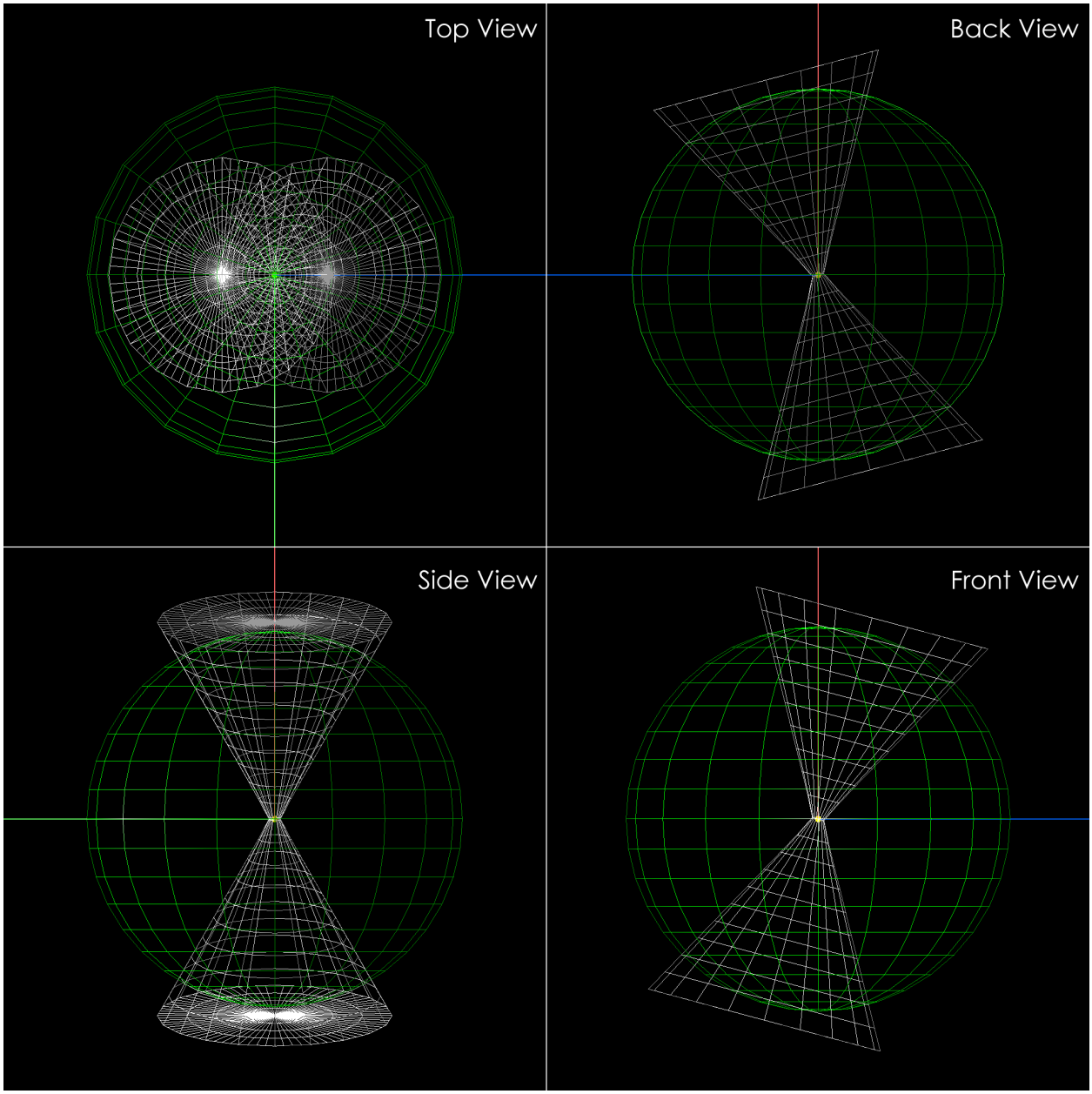

Fig. 4.— Mesh model of the Red Rectangle showing the geometry of the system. Each panel represents the model as seen from a different perspective. The model consists of two components, a sphere (green) and a bi-conical cavity (white). The density profile of each component is not illustrated (see Figure 5) and the colors are used simply to distinguish components.

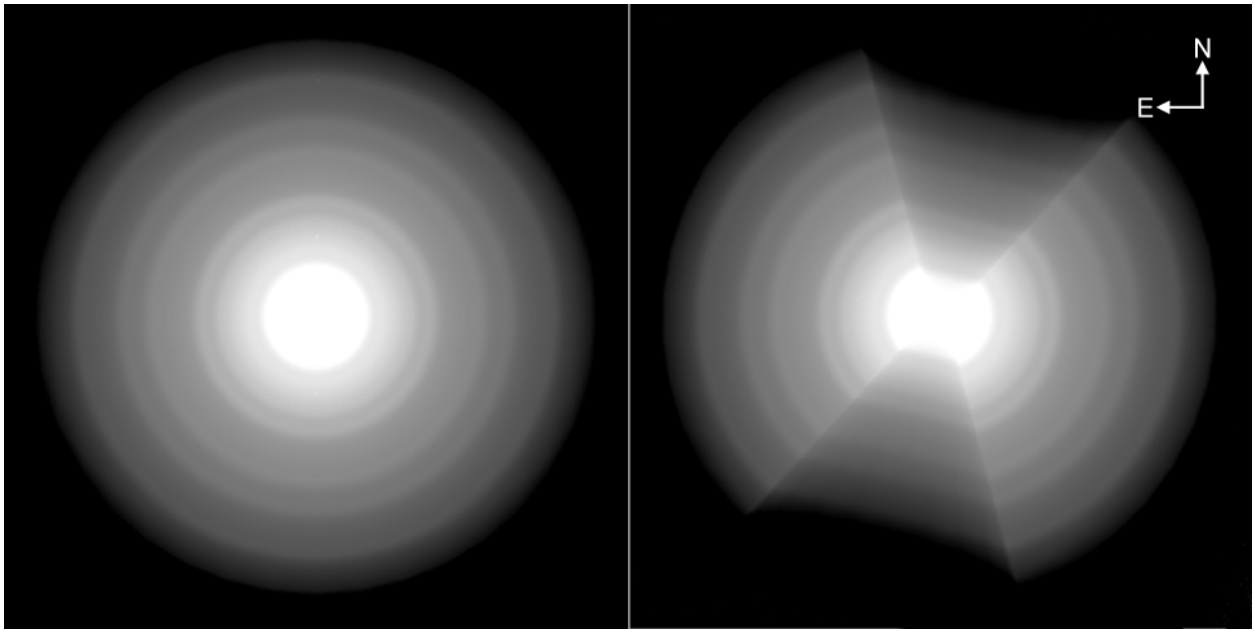

Fig. 5.— Integrated density distribution of the RR model. The brightness in the images is proportional to the density. The panel on the left shows the density within the sphere without the evacuating cavity. The panel on the right shows the density profile of the sphere with the bi-cone cavity. The image on the right shows clearly how a dense torus is naturally produced in this model. The images are shown in LOG scale.

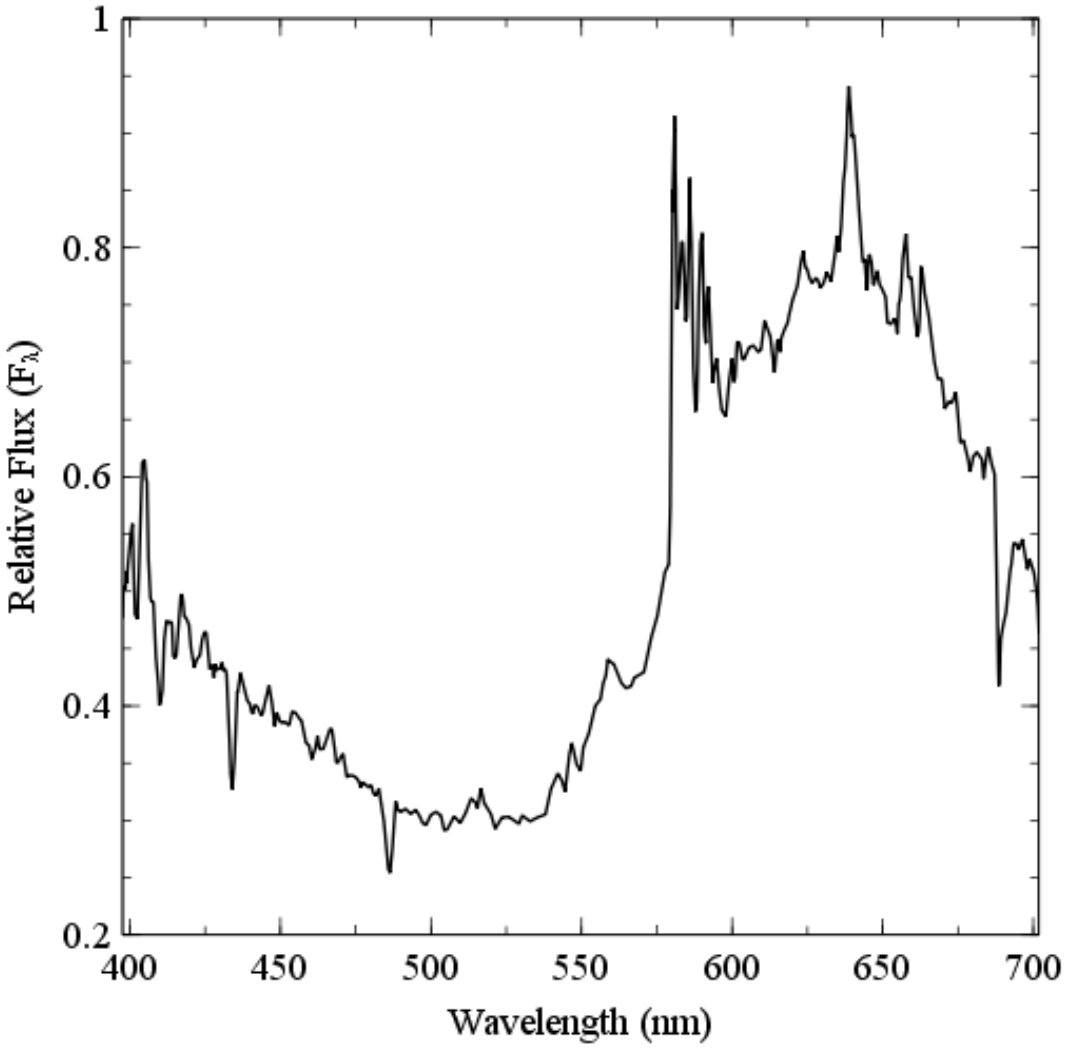

Fig. 6.— RR nebular spectrum 10" N of the central star at a resolution of 1 nm from Schmidt et al. (1980). The ERE is dominant at wavelengths longer than 540 nm whereas scattering dominates from 400 nm to 540 nm.

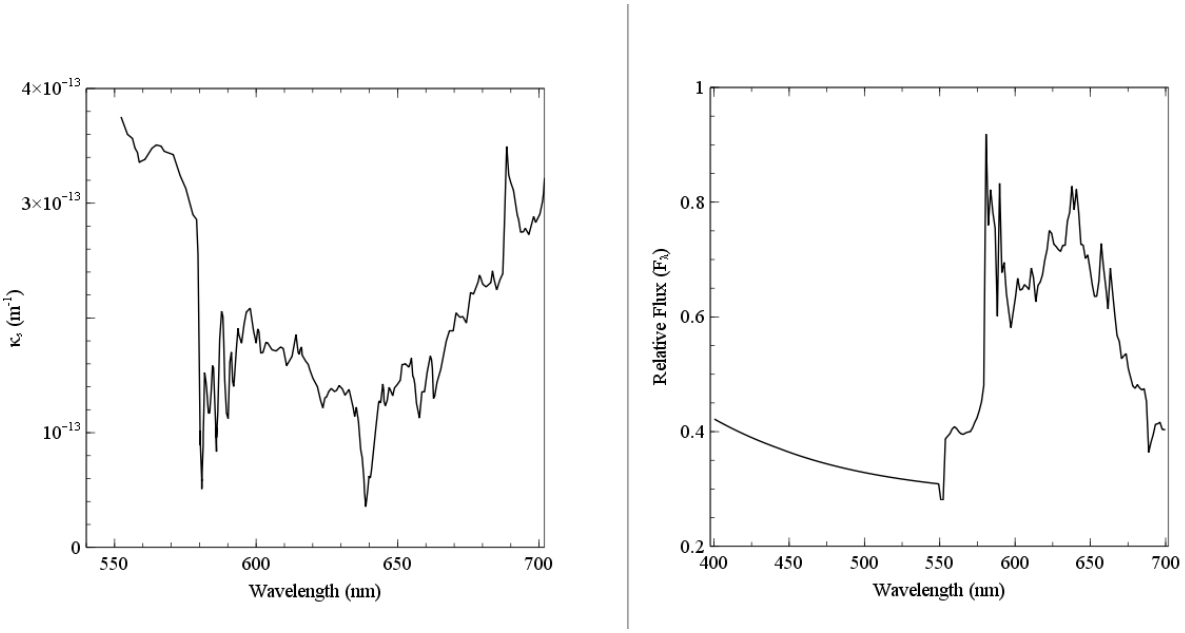

Fig. 7.— Left: Model ERE component scattering coefficients at wavelengths between 540 nm and 700 nm. Right: Model spectrum of the RR over 400 nm 700 nm (including contribution from silicate dust scattering). The scattering coefficients for the ERE were artificially selected to reproduce the spectrum in Figure 6.

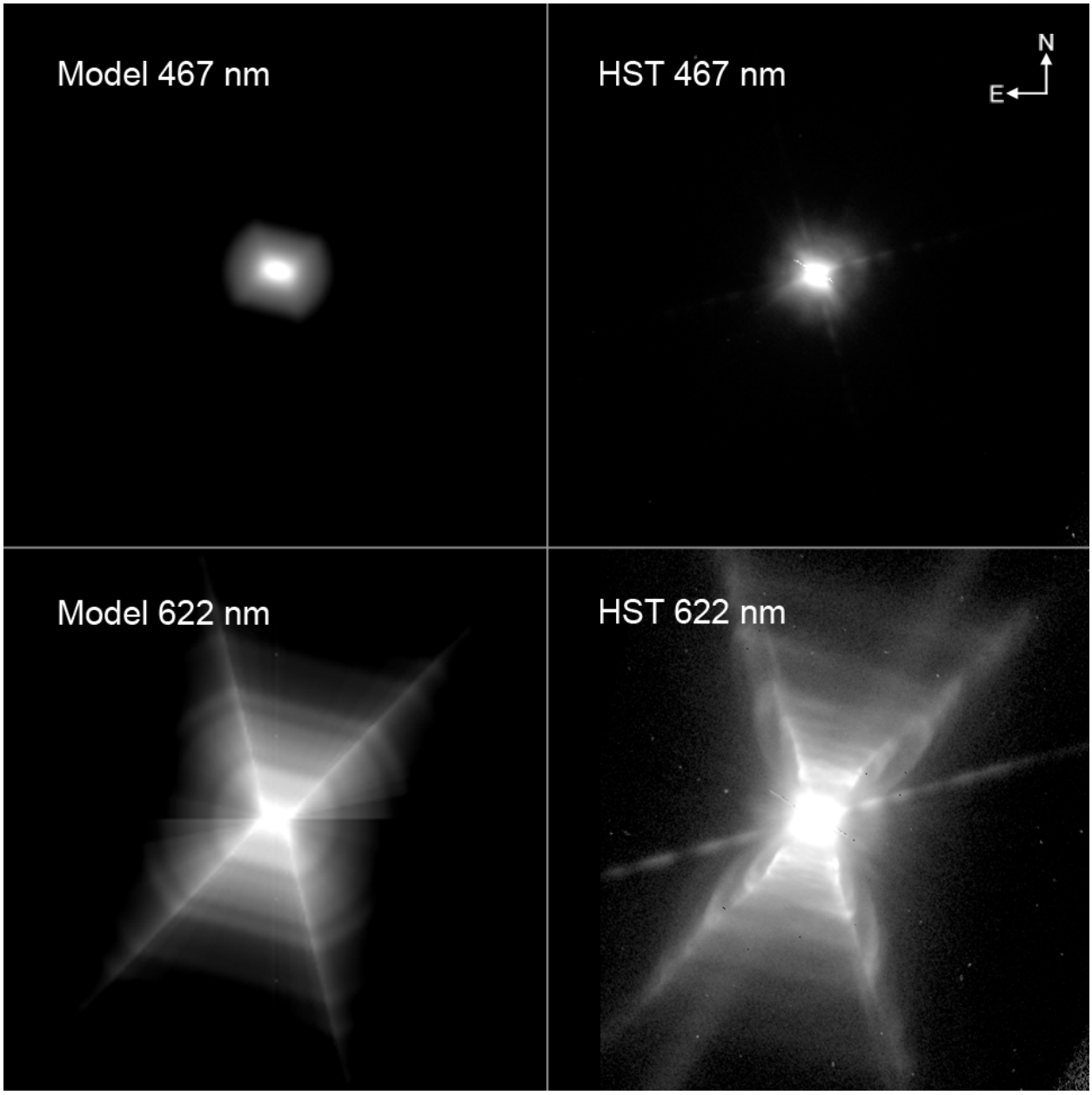

Fig. 8.— The top row shows the comparison between the SHAPE model (at an inclination of 0°) and HST image at 467 nm (HST F467M filter) and the bottom row shows the comparison at 622 nm (HST F662W filter). All images are displayed in a LOG scale. At the smaller wavelengths where scattering is dominant, only a spherical halo with a bright core is detected. At longer wavelengths dominated by the ERE, the morphology is much more complex. All images span 24" x 24". (HST image credit: PI Van Winckel, GO7297, Hubble Archives)

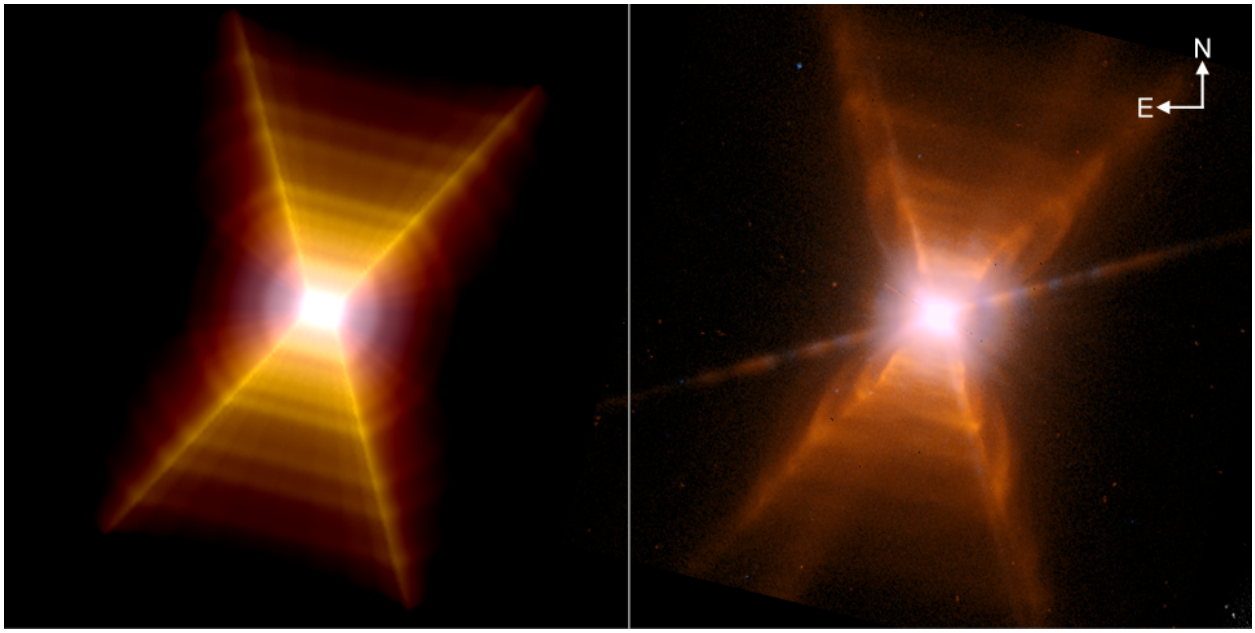

Fig. 9.— The left panel shows the SHAPE model of the Red Rectangle with an inclination of 0°. The image was rendered from 400 nm (blue) to 700 nm (red). The right panel is the HST image of the RR Nebula consisting of images from the F467M (467 nm), F588N (588 nm) and F622N (622 nm) filters of the PC detector. The color scale is the same as the model image. Both images are displayed in a LOG scale.

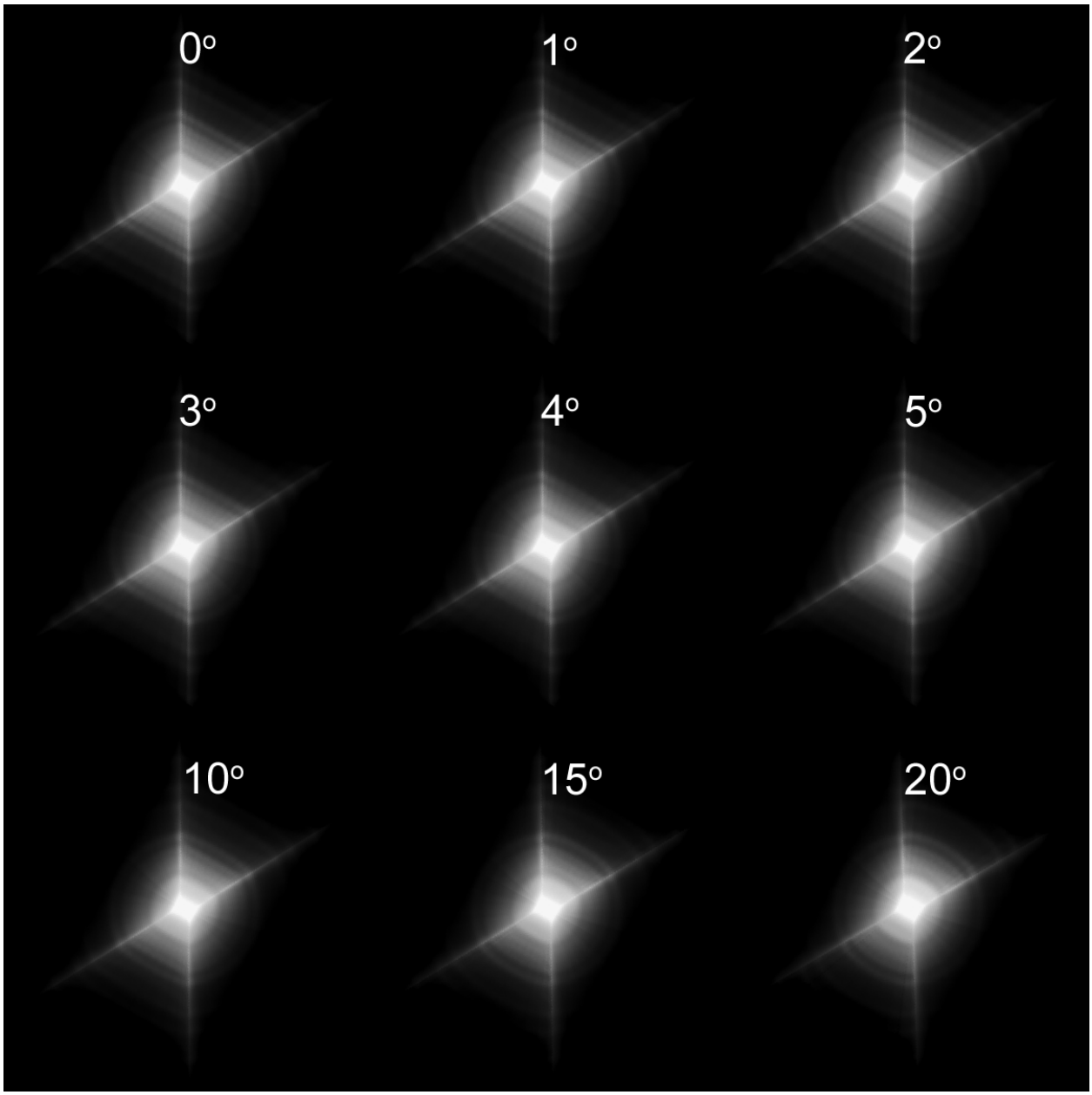

Fig. 10.— Model image of the RR at several different inclination angles (indicated above each image). As the inclination increases, the "ladder rungs" become arcs and the bright knots disappear. Each image is displayed in a LOG scale.

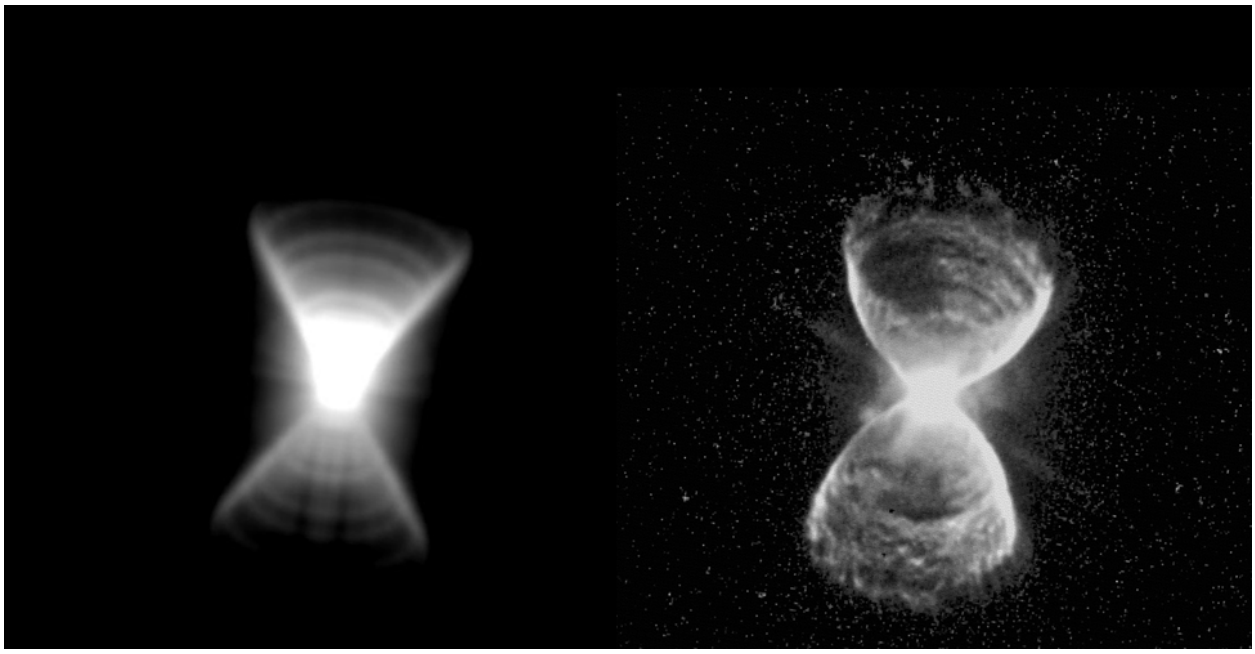

Fig. 11.— The left panel shows a model image of the RR at an inclination angle of 30°. The right panel shows the HST image of Hb12 (Kwok et al. 2007). The etchings seen in the RR may also explain those seen in Hb12 and other PNs with similar morphology.